IEEE Access
Multidisciplinary ⋮ Rapid Review ⋮ Open Access Journal

Received November 20, 2020, accepted December 6, 2020, date of publication December 30, 2020, date of current version March 1, 2021.

Digital Object Identifier 10.1109/ACCESS.2020.3048152

Broadband Athermal Waveguides and Resonators With Low Anomalous Dispersion

LIJUAN XU[1,2], YUHAO GUO[1], JING WANG[1], ZHAOHONG HAN[3], HENAN LIU[1], JURGEN MICHEL[3], LIONEL C. KIMERLING[3], (Life Member, IEEE), AND LIN ZHANG[1]

[1]Key Laboratory of Opto-electronic Information Technical Science of Ministry of Education, Key Laboratory of Integrated Opto-electronic Technologies and Devices in Tianjin, School of Precision Instruments and Opto-electronics Engineering, Tianjin University, Tianjin 300072, China
[2]School of Electronic Engineering, Tianjin University of Technology and Education, Tianjin 300222, China
[3]Microphotonics Center, Department of Materials Science and Engineering, Massachusetts Institute of Technology, Cambridge, MA 02139, USA

Corresponding author: Lin Zhang (lin_zhang@tju.edu.cn)

This work was supported in part by NSFC under Project 61775164 and Project 61775165; and in part by the Projects the fund of Tianjin University of Technology and Education under Grant KJ1921

ABSTRACT To mitigate the temperature sensitivity of photonic devices, materials with a negative thermo-optical coefficient (TOC) are integrated to optical waveguides. However, previously reported waveguides are made athermal at only one wavelength. In this paper, we theoretically propose a new broadband athermal waveguide, which consists of TiO_2 with a negative TOC and SiC with a positive TOC in its core. This composite core shows a near-zero broadband effective TOC, i.e., $\pm 1 \times 10^{-6}$/K over a 780-nm bandwidth from 1280 to 2060 nm. Furthermore, it also has low anomalous dispersion, from 66 to 329 ps/nm/km in the same wavelength range. This new athermal waveguide, when used to form microresonators, enables us to achieve broadband nonlinear applications with negligible intra-cavity thermal dynamics on a chip. We also show that the proposed waveguide can be tightly bent without suffering from a large bending loss/substrate leakage, which is suitable for dense integration.

INDEX TERMS Integrated optics, waveguides, microresonators, athermal devices, temperature sensitivity.

I. INTRODUCTION

Photonic integrated circuits have been intensely investigated in recent years [1]. Photonic devices suffer from a thermal drift of performance, especially for active or resonator-based devices. For example, a relatively large positive thermo-optical coefficient (TOC) in Si (1.8×10^{-4}/K [2]) remains a serious concern to the community of integrated photonics. Athermal waveguides and resonators [2]–[12] have been reported, using optical materials (polymer [3]–[8] or TiO_2 [2], [9]–[12]) with a negative TOC to balance the positive TOC in the waveguide core. A polymer cladding may have a low decomposition temperature and long-term stability issue, while TiO_2 is very attractive. It is noted that, in most cases, the athermal property has been achieved at only one wavelength [2]–[12], which is not adequate for WDM or wideband nonlinear applications. It would be desirable to achieve athermal operation for photonic devices over a wide band.

The associate editor coordinating the review of this manuscript and approving it for publication was Md Selim Habib.

Recently, a new waveguide structure [13] has been proposed for broadband athermal operation over a bandwidth of >300 nm, which has two claddings as shown in Fig. 1(a): one with a negative material TOC is closer to the waveguide core, while the other with a positive TOC corrects the wavelength dependence of the effective TOC. The dual-cladding waveguide has roughly half of modal power in the claddings to balance materials' TOCs, causing dramatic field expansion as wavelength increases and thus strong waveguide dispersion around −3600 ps/nm/km.

In fact, dispersion is an important property for a resonator when it is used for WDM applications. Due to dispersion, the resonance peaks of a cavity are not equally spaced in frequency domain, and the uniformity of free spectral ranges (FSRs) over a wide bandwidth is determined by intra-cavity dispersion [14]. If not controlled well, the dispersion can induce a difference of adjacent FSRs even more than a resonance linewidth, which is not suitable for WDM applications.

Moreover, dispersion is essential in nonlinear optics, e.g., for broadband parametric amplification, wavelength conversion, supercontinuum and frequency comb generation.

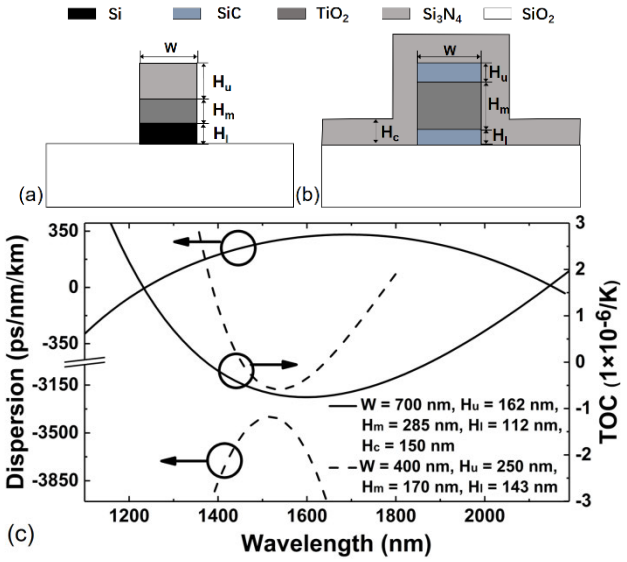

FIGURE 1. (a) The structure of broadband athermal waveguide [13]. (b) The waveguide structure of this paper. The TiO_2 layer is between two SiC layers. The cladding is Si_3N_4 and the substrate is SiO_2. (c) The dispersion properties and the effective TOCs of the waveguides (a) and (b).

For wideband phase matching, dispersion engineering typically aims to provide a small anomalous dispersion with one or more zero-dispersion wavelengths (ZDWs) [15], [16]. A flat and low dispersion has been obtained using dispersion-flattening with four ZDWs [17]–[22]. Recently, microresonator-based nonlinear devices [23]–[25] have become highly attractive, which are enabled via dispersion engineering as well as significant intra-cavity power buildup and thus strong nonlinearity. As a result, it is featured by slowly evolving thermal dynamics, which is viewed as a detrimental effect [26] and causes uncertainty in device performance. It would be highly desirable to obtain an athermal resonator over a wide band where dispersion is simultaneously engineered. However, this remains quite challenging.

In this work, we propose a novel waveguide to achieve both broadband athermal and low-dispersion properties simultaneously for the first time. It has a small effective TOC within $\pm 1 \times 10^{-6}$ /K over a 780-nm-wide bandwidth, from 1280 nm to 2060 nm. Its unique feature is a relatively small anomalous dispersion, from 66 to 329 ps/nm/km, over the same spectral range, which is suitable for wideband nonlinear parametric interactions with phase matching.

II. PRINCIPLE AND MATERIAL CHOICE

In principle, for athermal operation, mode field distribution should be balanced between positive-TOC and negative-TOC materials. Conventionally, athermal waveguides reach such a balance between waveguide core and cladding [2]–[12], but, as wavelength increases, the guided mode always expands more into the cladding, which causes that the athermal property only occurs at a single wavelength [2]–[12]. Generally speaking, the effective TOC of an athermal waveguide can be expressed in Eq. (1).

$$\frac{dn_{eff}}{dT}(\lambda) = \Gamma_c(\lambda)\frac{dn_c}{dT}(\lambda) + \Gamma_{cl}(\lambda)\frac{dn_{cl}}{dT}(\lambda) + \Gamma_{sub}(\lambda)\frac{dn_{sub}}{dT}(\lambda) \quad (1)$$

where $dn_c/dT(\lambda)$, $dn_{cl}/dT(\lambda)$, and $dn_{sub}/dT(\lambda)$ represent the material TOCs of waveguide core, cladding and substrate, respectively, and accordingly $\Gamma_c(\lambda)$, $\Gamma_{cl}(\lambda)$ and $\Gamma_{sub}(\lambda)$ are the power confinement factors of the waveguide mode. Typically, the material TOCs remain almost unchanged [27], [28] over a wavelength band of interest and the spectral dependence is ignored [2]–[12], while the confinement factors monotonically vary with wavelength. Therefore, the effective TOC becomes zero at only one wavelength.

In contrast, the broadband athermal waveguide in [13] has two claddings, as shown in Fig. 1(a). The lower cladding is used to balance the thermal properties at short wavelengths, while the upper cladding to correct the thermal properties at long wavelengths. This way, the waveguide core has to be small so that the mode is "squeezed" out to the upper cladding at long wavelengths. In this design approach, the dispersion is normal and as strong as -3600 ps/nm/km (see the dash line in Fig. 1(c)), which is not good for WDM and broadband nonlinear applications. Note that all the design freedoms are used to produce broadband athermal properties [13], and it becomes very challenging to tailor dispersion simultaneously.

Here, we use a new design approach, in which dispersion engineering and athermalization are separated to a certain extent. As shown in Fig. 1(b), waveguide core has two types of materials with the opposite TOCs but similar linear refractive indices. This means that the core is roughly balanced in terms of thermal properties, and the cladding is used to tailor dispersion [15]. This enables to use relatively fewer parameters to achieve dispersion tailoring and athermalization over a wide band simultaneously. It is important to note that adding the coat will slightly change the effective TOC and its wavelength dependence, but they can finally be corrected back by small modifications of core dimensions. Note that SiC has stronger Kerr nonlinearity than Si_3N_4. Although Si has even larger nonlinearity, the Si waveguide suffers from two-photon absorption over the wavelength range of interest. Thus, we consider using SiC for future use of this device for nonlinear applications. We also note that TiO_2 has negligible two-photon absorption around 1550 nm wavelength. It is important to emphasize that, although dispersion and athermalization are separated conceptually in the initial design, one has to jointly consider both in every step of dimension tailoring, because making dispersion and TOC both satisfactory (low and flat) over such a wide wavelength range is very challenging.

In our work, the presented waveguide has a TiO_2 layer with a negative TOC between two SiC layers with a positive TOC, as shown in Fig. 1(b). The cladding is Si_3N_4 and the substrate is SiO_2 which is 3 μm and silica-on-silicon-substate, both

with positive TOCs. We consider the quasi-TE mode, and its effective indices are obtained using a mode solver. All material dispersions [29]–[31] measured before are taken into account. TiO_2 and SiC have the refractive indices of around 2.4 and 2.6, which are close to each other.

For Si_3N_4, we use the following Sellmeier equation [29]:

$$n^2(\lambda) = 1 + C_1\lambda^2/(\lambda^2 - \lambda_1^2)$$

where $C_1 = 2.8939$ and $\lambda_1 = 0.13967\mu$m.

For SiC, we use the following Sellmeier equation [30]:

$$n^2(\lambda) = 1 + C_1\lambda^2/(\lambda^2 - C_2^2) + C_3\lambda^2/(\lambda^2 - C_4^2)$$

where $C_1 = 5.58245, C_2 = 0.1625394, C_3 = 2.468516, C_4 = 11.35656$.

We use the following Sellmeier equation for TiO_2 [31]:

$$n^2(\lambda) = E_d E_{owd}/(E_{owd}^2 - E^2 + 1)$$

where $eV = 1.602 \times 10^{-19}, E_d = 23.8$, $E_{owd} = 5.8$, $h = 6.626 \times 10^{-34}, E = hc/eV/(\lambda \times 10^{-6})$.

Group velocity dispersion, $D = -(c/\lambda) \cdot (d^2n_{eff}/d\lambda^2)$, is calculated, where n_{eff} is the effective index of the mode, and c and λ are the speed of light and wavelength in vacuum, respectively. The material TOCs of Si_3N_4, TiO_2, SiC, and SiO_2 are 2.45×10^{-5}/K [32], -1×10^{-4}/K [28], 1×10^{-4}/K [33], and 1×10^{-5}/K [2], respectively. More details about the materials are in Discussion section. In simulations, we set the mesh size in Si_3N_4, TiO_2, SiC, and SiO_2 to be 20, 40, 20 and 100 nm, and perfectly matched layer (PML) is 6 μm away from the waveguide, with a mesh size of 100 nm in it. To calculate the dispersion profile of the modes, we use a wavelength step of 20 nm, which has enough accuracy as confirmed in [17].

III. RESULT

The dimension parameters are the following: width $W = 700$ nm, upper height $H_u = 162$ nm, middle height $H_m = 285$ nm, lower height $H_l = 112$ nm and coated Si_3N_4 height $H_c = 150$ nm. Using this structure shown in Fig. 1(b), the broadband athermal property is found with an effective-TOC variation of $\pm 1 \times 10^{-6}$/K over a 780-nm bandwidth (1280 to 2060 nm) which is more than twice larger than that in [13]. The two zero-TOC wavelengths are 1380 and 1860 nm, and the TOC valley is at 1600 nm. A relatively flat and low dispersion profile is produced using a conformal Si_3N_4 coat layer [15]. The obtained dispersion is from 60 to 329 ps/nm/km from 1280 to 2060 nm, the same wavelength range as above. Two ZDWs are found at 1230 and 2150 nm, respectively. This amount of anomalous dispersion is usable for nonlinear parametric processes [23]–[25].

Mode field distributions at different wavelengths are shown in Fig. 2(a). The mode has more power in the upper SiC layer initially because $H_u > H_l$, and it accumulates in TiO_2 more and more as wavelength increases. At long wavelengths, the mode expands to the lower SiC layer and the Si_3N_4 coat with positive TOCs. As shown in Fig. 2(b),

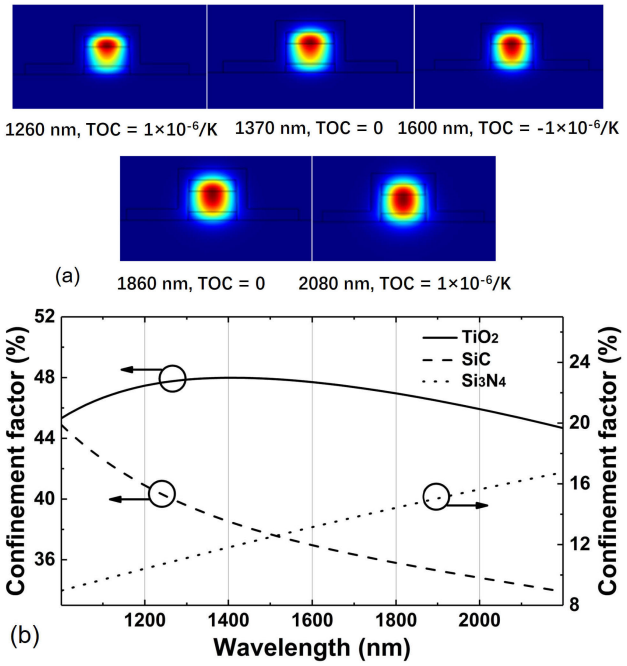

FIGURE 2. (a) Modal field distributions at different wavelengths. (b) Mode confinement factors in TiO_2 (solid line), SiC (dashed line) and Si_3N_4 (dotted line).

the mode confinement factor in TiO_2 has the maximum value at 1400 nm, but the effective TOC has its smallest value at 1600 nm. This can be explained as follows. Below 1400 nm, the effective TOC is positive because the mode confinement factor in the positive-TOC layers, the upper and lower SiC and coat Si_3N_4, is more than that in the negative-TOC TiO_2. From 1400 to 1600 nm, because the confinement factor in SiC decreases faster than in TiO_2, the effective TOC becomes negative and reaches the smallest value of -1×10^{-6}/K at 1600 nm as shown in Fig. 1(c). Then, the mode extends into the lower SiC and the coat more, making the effective TOC positive again. It is important to note that the design approach regarding the separation of dispersion engineering and athermalization mentioned above is conceptual. In fact, the Si_3N_4 coat would slightly affect the effective TOC as well, although its influence can be easily corrected by tailoring core dimensions.

The effects of structural parameters on the athermal and dispersion properties are examined by changing each of them around the optimum values, while the other parameters are kept the same. First, the dependence of the dispersion and the effective-TOC properties on the waveguide width is seen in Fig. 3(a). We calculate the curves for different widths ranging from 690 to 710 nm. The dispersion and effective TOC are almost the same in its shape and slope. At 1600-nm wavelength, the dispersion value decreases from 319 to 314 ps/nm/km and the effective TOC decreases from -6.8×10^{-7} to -8.2×10^{-7}/K as the width increases from 690 to 710 nm. This is because the width variation in the horizontal direction has almost no influence on the power ratio of the mode in positive-TOC and negative-TOC

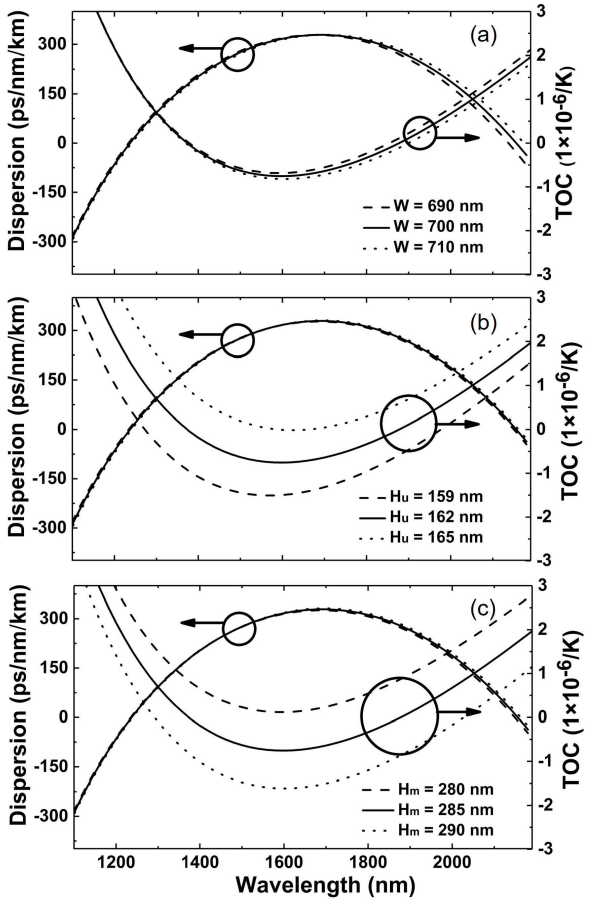

FIGURE 3. Dispersion and effective-TOC curves change with (a) width, (b) upper SiC height, (c) TiO_2 height.

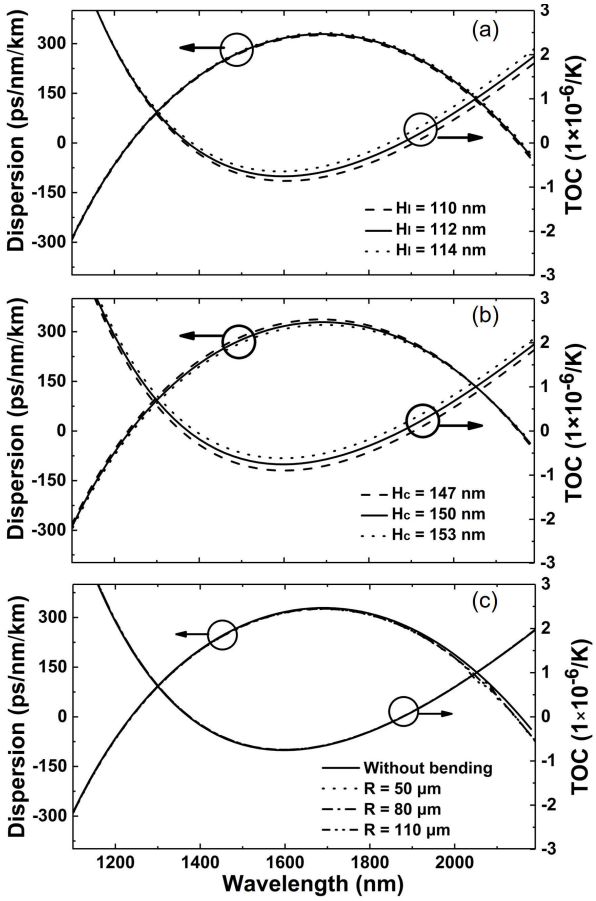

FIGURE 4. Dispersion and effective-TOC curves change with (a) lower SiC height, (b) coated Si_3N_4 thickness, and (c) bending radius.

materials in the vertical direction, which determines the effective TOC.

When the upper SiC height, H_u, is increased from 159 to 165 nm, the dispersion slightly increases from 316 to 317 ps/nm/km, and the effective TOC increases from -1.4×10^{-6} to -7.6×10^{-9}/K at 1600-nm wavelength, as shown in Fig. 3(b). As H_u is increased, the mode moves more into the positive-TOC material, so the effective TOC increases. Similarly, when the height of TiO_2 is increased from 280 to 290 nm, the dispersion increases slightly from 315 to 318 ps/nm/km, and the effective TOC decreases from 1.1×10^{-7} to -1.6×10^{-6}/K at 1600-nm wavelength in Fig. 3(c), because the mode in negative-TOC material is raised, so the curve of the effective-TOC moves down entirely. Because less mode is confined in the lower SiC layer, the effective TOC does not change much with the height of SiC, H_l. For example, at 1600-nm wavelength, when H_l is increased from 110 to 114 nm, the dispersion increases from 314 to 320 ps/nm/km, and the effective TOC slightly increases, as shown in Fig. 4(a).

To obtain flat and low dispersion, the multilayer structure is conformally coated with Si_3N_4 [15]. The coating layer affects dispersion and the effective TOC as illustrated in Fig. 4(b). At 1600-nm wavelength, when the thickness is increased from 147 to 153 nm, the dispersion is decreased from 326 to 308 ps/nm/km and the effective-TOC is increased from -8.9×10^{-7} to -6.1×10^{-7}/K. When the proposed waveguide is used to form a ring resonator, the influence of bending radius (R) on dispersion and the effective TOC is shown in Fig. 4(c). The dispersion and effective TOC have a negligible change as the radius increases from 50 to 110 μm.

From above, the effective TOC changes with the upper SiC and TiO_2 heights, as shown in Fig. 3(b) and Fig. 3(c). This requires careful calibration of the film deposition rate in device fabrication. When width, lower SiC height and coated Si_3N_4 height change, the effective TOC varies slightly. The reason can be explained from the mode distributions shown in Fig. 2. The mode is mainly confined in upper SiC layer and TiO_2 layer, so they have a dominant influence on the ratio of the mode in the positive-TOC and negative-TOC materials. The effective TOC changes negligibly when the other structural parameters change.

Since the effective TOC is more sensitive to the variations of the upper SiC height and the TiO_2 height, we examine its dependence on those at the zero-TOC wavelengths, i.e., 1380 and 1860 nm. As shown in Fig. 5, the effective TOC moves within a range of $\pm 20 \times 10^{-6}$ /K, when the upper SiC height is changed from 122 to 202 nm and the TiO_2 height

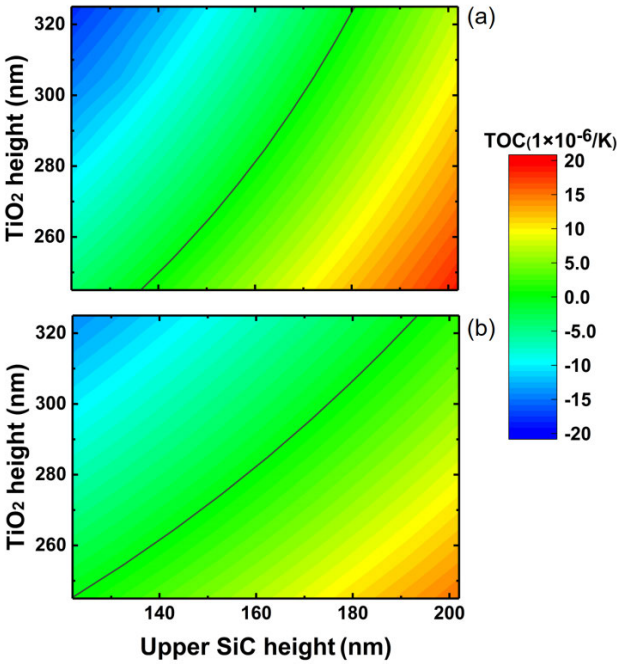

FIGURE 5. The effective TOC varies with the upper SiC height and the TiO_2 height at (a) 1380-nm and (b) 1860-nm wavelengths. Solid lines are for zero-TOCs.

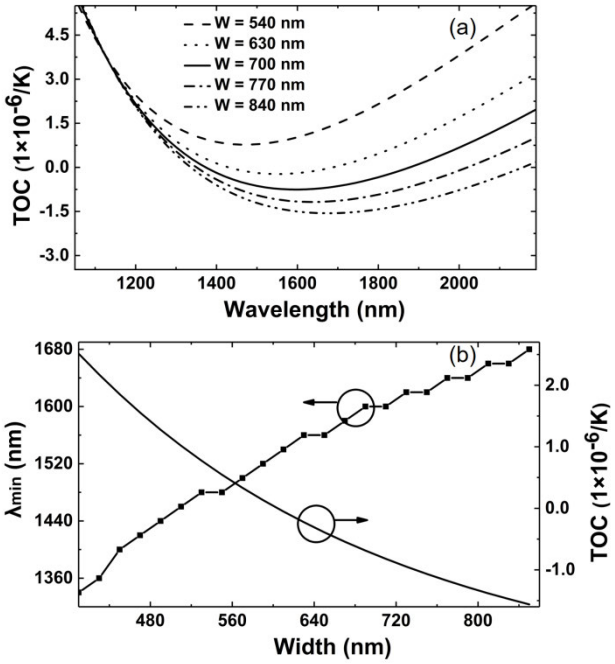

FIGURE 6. (a) Dispersion and effective TOC change with width; (b) The smallest effective TOC and the corresponding wavelength shift with the width.

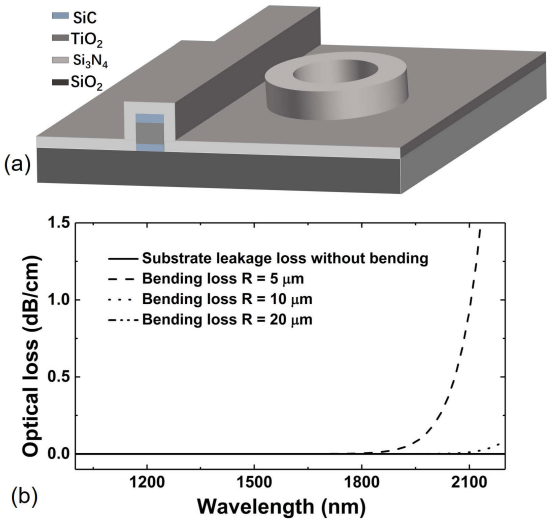

FIGURE 7. (a) Microresonator based on the proposed waveguide; (b) The substrate leakage loss of the proposed waveguide without bending and the bending loss with different radii.

is from 245 to 325 nm. The solid lines in Fig. 5 represent the cases where the effective TOC is zero. Compared to the data at 1860 nm, the line at 1380 nm changes faster, because the confinement factor is more sensitive to the change in the upper SiC height at short wavelengths than at long wavelengths. Nevertheless, we can still obtain a quite low TOC when changing the heights of SiC and TiO_2 simultaneously in a certain range.

As the waveguide width increases, the TOC curves move down, as shown in Fig. 6(a), and we note that the mode in the middle TiO_2 layer increases more than in SiC. The smallest effective TOC decreases from 2.5×10^{-6} to -1.5×10^{-6}/K and moves from 1340 to 1680 nm wavelength, as the width increases from 410 to 850 nm, as shown in Fig. 6(b). We can obtain a wider bandwidth through increasing the width and a small change in the Si_3N_4 coat thickness.

The modal field in the waveguide extends to the substrate as wavelength increases, as shown in Fig. 2(a), and thus substrate leakage becomes more significant at long wavelengths especially when the waveguide is tightly bent. When used in microresonators (as shown in Fig. 7(a)), the proposed waveguide has a negligible bending loss when the bending radius is 10 μm or more, as shown in Fig. 7(b). This is much better than that in [13], proving that the proposed waveguide with a layered core is more suitable for dense integration than the reported waveguide with multiple claddings in [13].

The temperature-dependent wavelength shift (TDWS) in a microresonator [8] is determined by Eq. (1)

$$\partial\lambda_0/\partial T = (\lambda_0/n_g) \times (\partial n_{eff}/\partial T) \quad (2)$$

where λ_0 is the resonance wavelength, and n_g is the group index of the mode. A variation of TDWS within $\pm$0.5 pm/K in the wavelength range from 1280 to 2000 nm is obtained, as shown in Fig. 8. Note that the TDWS of a silicon waveguide is roughly 110 pm/K [34], an improvement of two orders of magnitude in thermal sensitivity. Around 1550 nm as an example, such a TDWS is corresponding to 63 MHz/K, which is less than the resonance linewidth of a high-Q cavity ($Q = 3 \times 10^6$). In microresonator-based frequency comb generation, thermally induced resonance shift is 14-100 pm [26], [35], [36], and this can be dramatically reduced to about 1 pm over the whole 720-nm bandwidth if using the proposed waveguide.

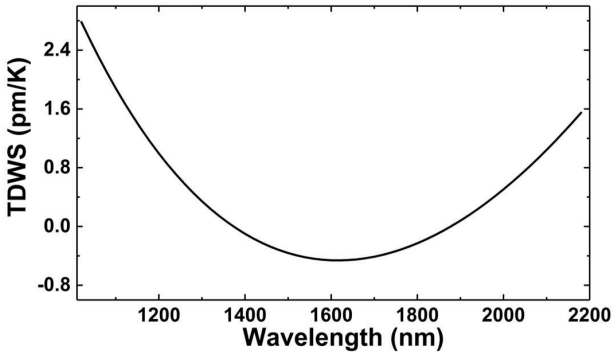

FIGURE 8. The TDWS of a microresonator formed using the proposed waveguide, which is ±0.5 pm/K in the wavelength from 1280 to 2000 nm.

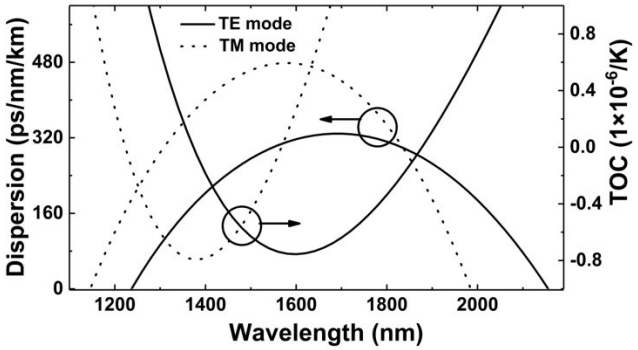

FIGURE 9. Dispersion and effective-TOC curves of TE mode (solid line) and TM mode (dashed line).

IV. DISCUSSION

We note that in principle material TOC varies with temperature and wavelength [37]. To experimentally verify the proposed broadband athermal device, complete measurement of material TOCs are needed. In addition, as temperature changes, different material layers may become stressed due to thermal expansion [38], which affects both TOC and dispersion. However, it is important to emphasize that all the above issues could be viewed as higher-order perturbation [38] in waveguide design in future and can be corrected by slightly changing dimensional parameters, when a temperature/wavelength range of interest is specified.

In device fabrication, atomic layer deposition (ALD) for TiO_2 is preferred [31] for better thickness control, which produces amorphous TiO_2, and state of the art ALD machines (e.g., from BENEQ) exhibit short cycle times and fast deposition. Plasma enhanced chemical vapor deposition can be used for other materials, and small thickness variation can be pre-calibrated [39] and taken into account in the next round of device design and fabrication. Although deposited Si_3N_4 layer may have N-H bond absorption, it is noted that only a small fraction of optical modal power is in that layer.

Although in this paper we use TE mode to obtain broadband and small effective TOC and low anomalous dispersion, we also find that one can have it for a TM mode, as shown in Fig. 9. The near-zero effective TOC is obtained within $\pm 1 \times 10^{-6}$/K over a 520-nm bandwidth from 1160 to 1680 nm for the TM mode, which is narrower than the TE mode.

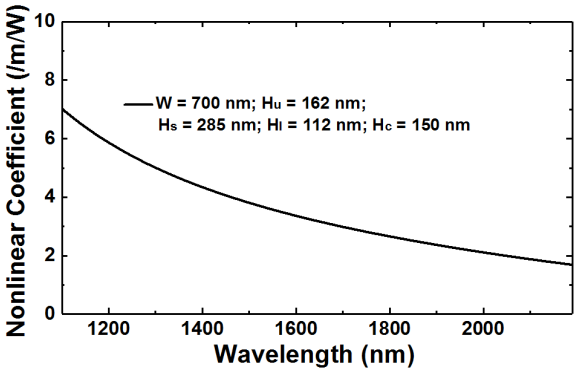

FIGURE 10. The nonlinear coefficient for the presented waveguide.

The dispersion is varying from 33 to 478 ps/nm/km at the same bandwidth. The dimension parameters are given as follows: width W = 700 nm, upper height H_u = 200 nm, middle height H_m = 220 nm, lower height H_l = 112 nm and coated Si_3N_4 height H_c = 150 nm. It is thus proved that the proposed athermalization scheme can be generally applicable to both TE and TM modes, which can expand the use of the proposed athermal waveguides.

For resonator-based nonlinear applications, with the greatly reduced TDWS, one may not need a tunable pump laser anymore to follow the resonance shift due to a thermal drift [26], [35], [36], as a large amount of power is injected into the cavity. Removing the need for an on-chip tunable pump laser would significantly mitigate the challenges to build a fully integrated nonlinear system.

We consider using SiC for future nonlinear applications because of its strong Kerr nonlinearity (5.9×10^{-17}cm^2/W). Figure 10 shows the high nonlinear coefficient γ decreases with wavelength. Note that the considered wavelength range for the presented waveguide is beyond half-bandgap wavelength, and two-photon absorption can thus be ignored. The materials are all in transparency window, which are very suitable for microresonators.

V. SUMMARY

We have proposed a novel waveguide that exhibits temperature-insensitive properties over a 780-nm-wide band, from 1280 to 2060 nm, with a near-zero TOC within $\pm 1 \times 10^{-6}$/K. The unique feature of this waveguide is its small anomalous dispersion from 66 to 329 ps/nm/km, in the same spectral range. The device can be used for nonlinear applications using microresonators. This athermalization scheme is expected to enable practical monolithically integrated photonic devices.

REFERENCES

[1] M. Hochberg and T. Baehr-Jones, "Towards fabless silicon photonics," *Nature Photon.*, vol. 4, no. 8, pp. 492–494, Aug. 2010.
[2] B. Guha, J. Cardenas, and M. Lipson, "Athermal silicon microring resonators with titanium oxide cladding," *Opt. Exp.*, vol. 21, no. 22, pp. 26557–26563, Oct. 2013.
[3] Y. Kokubun, S. Yoneda, and S. Matsuura, "Temperature-independent optical filter at 1.55 μm wavelength using a silica-based athermal waveguide," *Electron. Lett.*, vol. 34, no. 4, pp. 367–369, Feb. 1998.

[4] J.-M. Lee, D.-J. Kim, H. Ahn, S.-H. Park, and G. Kim, "Temperature dependence of silicon nanophotonic ring resonator with a polymeric overlayer," *J. Lightw. Technol.*, vol. 25, no. 8, pp. 2236–2243, Aug. 2007.
[5] W. N. Ye, J. Michel, and L. C. Kimerling, "Athermal high-index-contrast waveguide design," *IEEE Photon. Technol. Lett.*, vol. 20, no. 11, pp. 885–887, Jun. 2008.
[6] P. Alipour, E. S. Hosseini, A. A. Eftekhar, B. Momeni, and A. Adibi, "Athermal performance in high-Q polymer-clad silicon microdisk resonators," *Opt. Lett.*, vol. 35, no. 20, pp. 3462–3464, Oct. 2010.
[7] J. Teng, P. Dumon, W. Bogaerts, H. Zhang, X. Jian, M. Zhao, G. Morthier, and R. Baets, "Athermal Silicon-on-insulator ring resonators by overlaying a polymer cladding on narrowed waveguides," *Opt. Exp.*, vol. 17, no. 17, pp. 14627–14633, Aug. 2009.
[8] V. Raghunathan, W. N. Ye, J. Hu, T. Izuhara, J. Michel, and L. Kimerling, "Athermal operation of silicon waveguides: Spectral, second order and footprint dependencies," *Opt. Exp.*, vol. 18, no. 17, pp. 17631–17639, Aug. 2010.
[9] S. S. Djordjevic, K. Shang, B. Guan, S. T. Cheung, L. Liao, J. Basak, H.-F. Liu, and S. Yoo, "Cmos-compatible, athermal silicon ring modulators clad with titanium dioxide," *Opt. Exp.*, vol. 21, no. 12, pp. 13958–13968, Jun. 2013.
[10] F. Qiu, A. M. Spring, F. Yu, and S. Yokoyama, "Complementary metal–oxide–semiconductor compatible athermal silicon nitride/titanium dioxide hybrid micro-ring resonators," *Appl. Phys. Lett.*, vol. 102, no. 5, Feb. 2013, Art. no. 051106.
[11] F. Qiu, A. M. Spring, and S. Yokoyama, "Athermal and high-Q hybrid TiO_2–Si_3N_4 ring resonator via an etching-free fabrication technique," *ACS Photon.*, vol. 2, no. 3, pp. 405–409, Mar. 2015.
[12] T. Lipka, L. Moldenhauer, J. Müller, and H. K. Trieu, "Athermal and wavelength-trimmable photonic filters based on TiO_2-cladded amorphous-SOI," *Opt. Exp.*, vol. 23, no. 15, pp. 20075–20088, Jul. 2015.
[13] L. Q. He, H. N. Liu, Z. H. Han, K. Wada, J. Michel, A. Agarwal, L. C. Kimerling, G. F. Li, and L. Zhang, "Broadband athermal waveguides and resonators for datacom and telecom applications," *Photon. Res.*, vol. 6, no. 11, pp. 987–990, Nov. 2018.
[14] L. Zhang, Y. Yue, R. G. Beausoleil, and A. E. Willner, "Analysis and engineering of chromatic dispersion in silicon waveguide bends and ring resonators," *Opt. Exp.*, vol. 19, no. 9, pp. 8102–8107, Apr. 2011.
[15] X. Liu, W. M. J. Green, X. Chen, I.-W. Hsieh, J. I. Dadap, Y. A. Vlasov, and R. M. Osgood, "Conformal dielectric overlayers for engineering dispersion and effective nonlinearity of silicon nanophotonic wires," *Opt. Lett.*, vol. 33, no. 24, pp. 2889–2891, Dec. 2008.
[16] L. Zhang, Y. Yue, Y. Xiao-Li, J. Wang, R. G. Beausoleil, and A. E. Willner, "Flat and low dispersion in highly nonlinear slot waveguides," *Opt. Exp.*, vol. 18, no. 12, pp. 13187–13193, Jun. 2010.
[17] L. Zhang, Y. Yue, R. G. Beausoleil, and A. E. Willner, "Flattened dispersion in silicon slot waveguides," *Opt. Exp.*, vol. 18, no. 19, pp. 20529–20534, Sep. 2010.
[18] P. W. Nolte, C. Bohley, and J. Schilling, "Tuning of zero group velocity dispersion in infiltrated vertical silicon slot waveguides," *Opt. Exp.*, vol. 21, no. 2, pp. 1741–1750, Jan. 2013.
[19] D. Castelló-Lurbe and E. Silvestre, "Inverse dispersion engineering in silicon waveguides," *J. Opt. Soc. Amer. B, Opt. Phys.*, vol. 31, no. 8, pp. 1829–1835, Aug. 2014.
[20] L. Xu, X. Ni, B. Liu, Y. Li, and M. Hu, "Ultraflat and low dispersion in a horizontal silicon nitride slot waveguide at near-infrared wavelengths," *Opt. Eng.*, vol. 55, no. 3, Mar. 2016, Art. no. 037109.
[21] Z. Jafari, L. Zhang, A. M. Agarwal, L. C. Kimerling, J. Michel, and A. Zarifkar, "Parameter space exploration in dispersion engineering of multilayer silicon waveguides from near-infrared to mid-infrared," *J. Lightw. Technol.*, vol. 34, no. 16, pp. 3696–3702, Aug. 15, 2016.
[22] Y. H. Guo, Z. Jafari, A. M. Agarwal, L. C. Kimerling, G. Li, L. Zhang, and J. Michel, "Bilayer waveguides for dispersion flattening with four zero-dispersion wavelengths," *Opt. Lett.*, vol. 41, no. 21, pp. 4939–4942, Nov. 2016.
[23] J. S. Levy, A. Gondarenko, M. A. Foster, A. C. Turner-Foster, A. L. Gaeta, and M. Lipson, "CMOS-compatible multiple-wavelength oscillator for on-chip optical interconnects," *Nature Photon.*, vol. 4, no. 1, pp. 37–40, Jan. 2010.
[24] F. Morichetti, A. Canciamilla, C. Ferrari, A. Samarelli, M. Sorel, and A. Melloni, "Travelling-wave resonant four-wave mixing breaks the limits of cavity-enhanced all-optical wavelength conversion," *Nature Commun.*, vol. 2, no. 1, pp. 1–8, May 2011.
[25] J. R. Ong, M. L. Cooper, G. Gupta, W. M. J. Green, S. Assefa, F. Xia, and S. Mookherjea, "Low-power continuous-wave four-wave mixing in silicon coupled-resonator optical waveguides," *Opt. Lett.*, vol. 36, no. 15, pp. 2964–2966, Aug. 2011.
[26] C. Y. Bao, Y. Xuan, J. A. Jaramillo-Villegas, D. E. Leaird, M. Qi, and A. M. Weiner, "Direct soliton generation in microresonators," *Opt. Lett.*, vol. 42, no. 13, pp. 2519–2522, Jul. 2017.
[27] J. Joo, J. Park, and G. Kim, "Cost-effective 2 × 2 silicon nitride Mach-Zehnder interferometric (MZI) thermo-optic switch," *IEEE Photon. Technol. Lett.*, vol. 30, no. 8, pp. 740–743, Apr. 15, 2018.
[28] M. R. Saleem, P. Silfsten, S. Honkanen, and J. Turunen, "Thermal properties of TiO_2 films grown by atomic layer deposition," *Thin Solid Films*, vol. 520, no. 16, pp. 5442–5446, Jun. 2012.
[29] L. Zhang, A. M. Agarwal, L. C. Kimerling, and J. Michel, "Nonlinear group IV photonics based on silicon and germanium: From near-infrared to mid-infrared," *Nanophotonics*, vol. 3, nos. 4–5, pp. 247–268, Aug. 2014.
[30] E. D. Palik, *Handbook of Optical Constants of Solids*. Sacramento, CA, USA: Academic, 1998, pp. 587–595.
[31] D. Saha, R. S. Ajimsha, K. Rajiv, C. Mukherjee, M. Gupta, P. Misra, and L. M. Kukreja, "Spectroscopic ellipsometry characterization of amorphous and crystalline TiO_2 thin films grown by atomic layer deposition at different temperatures," *Appl. Surf. Sci.*, vol. 315, no. 1, pp. 116–123, Oct. 2014.
[32] A. Arbabi and L. L. Goddard, "Measurements of the refractive indices and thermo-optic coefficients of Si_3N_4 and SiOx using microring resonances," *Opt. Lett.*, vol. 38, no. 19, pp. 3878–3881, Oct. 2013.
[33] F. G. Della Corte, M. E. Montefusco, L. Moretti, I. Rendina, and A. Rubino, "Study of the thermo-optic effect in hydrogenated amorphous silicon and hydrogenated amorphous silicon carbide between 300 and 500 k at 1.55 μm," *Appl. Phys. Lett.*, vol. 79, no. 2, pp. 168–170, Jul. 2001.
[34] K. Padmaraju, J. Chan, L. Chen, M. Lipson, and K. Bergman, "Thermal stabilization of a microring modulator using feedback control," *Opt. Exp.*, vol. 20, no. 27, pp. 27999–28008, Dec. 2012.
[35] P. H. Wang, J. A. Jaramillo-Villegas, Y. Xuan, X. X. Xue, C. Y. Bao, D. E. Leaird, M. H. Qi, and A. M. Weiner, "Intracavity characterization of micro-comb generation in the single-soliton regime," *Opt. Exp.*, vol. 24, no. 10, pp. 10890–10897, May 2016.
[36] H. Guo, M. Karpov, E. Lucas, A. Kordts, M. H. P. Pfeiffer, V. Brasch, G. Lihachev, V. E. Lobanov, M. L. Gorodetsky, and T. J. Kippenberg, "Universal dynamics and deterministic switching of dissipative Kerr solitons in optical microresonators," *Nat. Phys.*, vol. 13, no. 1, pp. 94–103, Sep. 2016.
[37] S. Q. Feng, K. Shang, J. T. Bovington, R. Wu, B. Guan, K.-T. Cheng, J. E. Bowers, and S. J. Ben Yoo, "Athermal silicon ring resonators clad with titanium dioxide for 1.3 μm wavelength operation," *Opt. Exp.*, vol. 23, no. 20, pp. 25653–25660, Sep. 2015.
[38] J. Bovington, R. Wu, K.-T. Cheng, and J. E. Bowers, "Thermal stress implications in athermal TiO_2 waveguides on a silicon substrate," *Opt. Exp.*, vol. 22, no. 2, pp. 661–666, Jan. 2014.
[39] J. Sun, "Toward accurate and large-scale silicon photonics," Ph.D. dissertation, Dept. Elect. Eng. Comput. Sci., Massachusetts Inst. Technol., Cambridge, MA, USA, Feb. 2013.

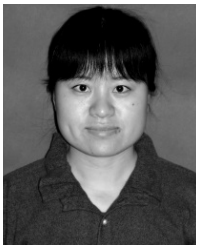

LIJUAN XU was born in Shandong, China, in 1980. She received the B.S. degree from Jilin University, Jilin, China, in 2004, and the M.S. degree in electronic science and engineering from Tianjin University, Tianjin, China, in 2007, where she is currently pursuing the Ph.D. degree in optical engineering.

She is also a Lecturer with the School of Electronic Engineering, Tianjin University of Technology and Education. Her current research interests include dispersion engineering in optical waveguides, athermal waveguide, and nonlinear optics in optical waveguides.

YUHAO GUO was born in Henan, China, in 1991. He received the B.S. degree in electronic science and engineering from Tianjin University, Tianjin, China, in 2015, where he is currently pursuing the Ph.D. degree in optical engineering.

He has published two articles. His research interests include dispersion engineering, frequency comb generation, supercontinuum generation, and metasurface.

JING WANG was born in Henan, China, in 1992. She received the B.S. degree in electronic science and engineering from Tianjin University, Tianjin, China, in 2015, where she is currently pursuing the Ph.D. degree in optical engineering.

She has published two articles. Her research interests include frequency comb generation, supercontinuum generation, and dispersion engineering.

ZHAOHONG HAN received the B.S. degree in materials science and engineering from Tsinghua University, Beijing, China, in 2011, and the Ph.D. degree from the Department of Materials Science and Engineering, Massachusetts Institute of Technology (MIT), in 2016, where he is working on Ge and Chalcogenide photonic devices.

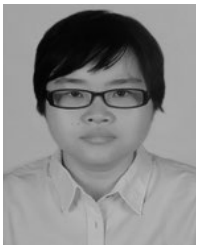

HENAN LIU was born in Tianjin, China, in 1987. She received the B.S. degree in electronic science and technology from Tianjin University, Tianjin, in 2010, and the Ph.D. degree in optical science and engineering from the University of North Carolina, Charlotte, NC, USA, in 2015.

From 2016 to 2017, she was a Postdoctoral Research Fellow with the Institute of Semiconductors, Chinese Academy of Sciences, Beijing, China. She is currently working as an Assistant Professor with the Key Laboratory of Opto-electronic Information Technology of Ministry of Education, School of Precision Instrument and Opto-electronics Engineering, Tianjin University. She has published nine articles. Her research interests include near-field optical manipulation, novel physics in nanostructures, and optical spectroscopy and characterization.

JURGEN MICHEL received the Diploma degre in physics from the University of Cologne, Cologne, Germany, and the Ph.D. degree in applied physics from the University of Paderborn, Paderborn, Germany.

He joined the Massachusetts Institute of Technology, Cambridge, in 1990, where he is currently a Principal Research Scientist with the Microphotonics Center. He was a Postdoctoral Member of the Technical Staff with AT&T Bell Laboratories. He has authored or coauthored more than 180 scientific articles. His current research interests include silicon-based photonic materials and devices and silicon-based photovoltaics.

LIONEL C. KIMERLING (Life Member, IEEE) received the B.S. degree in metallurgical engineering and the Ph.D. degree in materials science from the Massachusetts Institute of Technology (MIT), Cambridge, in 1965 and 1969, respectively.

He was formerly the Head of the Materials Physics Research Department, AT&T Bell Laboratories, Holmdel, NJ, USA. He is currently the Thomas Lord Professor of Materials Science and Engineering with MIT, where he is also the Director of the Materials Processing Center. He is involved in the field of electronic, optical, and optoelectronic materials. His current research interests include silicon processing, photovoltaic cells, environmentally benign integrated circuit manufacturing, and monolithic microphotonic devices and circuits.

LIN ZHANG received the B.S. and M.S. degrees (Hons.) from Tsinghua University, China, in 2001 and 2004, respectively, and the Ph.D. degree from the University of Southern California (USC), USA, in 2011.

He worked as a Postdoctoral Researcher with the Massachusetts Institute of Technology (MIT), USA. Since 2015, he has been a Professor with Tianjin University, China. He has published over 220 peer-reviewed journal articles and conference papers, including 20 invited papers, and two book chapters. He has five patents issued. His H-index is 30. His research interests include integrated nano-photonics, on-chip nonlinear ultrafast phenomena, micro-resonator devices and system applications, chip-scale optical interconnects, sensing, and photonic crystal fibers.

Dr. Zhang is a member of the IEEE Photonics Society and a Senior Member of the Optical Society of America (OSA). He received the Tianjin Youth 1000-Talent Award, in 2014, and the national Youth 1000-Talent Award and Peiyang Scholar - Outstanding Talent Oversea Award, in 2015.